Observations of Spectroscopic Binaries Epsilon Persei and HIP26736

A thesis presented in partial fulfilment of the requirements for the degree of Bachelor of Science

Katie Vasquez

Sc.B. Degree Candidate in Astrophysics

Faculty Advisor: Ian Dell'Antonio

Brown University Department of Physics

Providence RI

4/29/2020

Contents

List of Figures

Abstract

Observations of Spectroscopic Binaries Epsilon Persei and HIP26736

Spectroscopic binaries are an essential tool in astrophysics because they provide a simple method of determining the masses and radii of stars to high precision and accuracy. The proprieties of binary star systems are used in calibration of theoretical stellar models, to determine the distance of nearby galaxies, and other asteroseismology studies.

In this thesis, I use high resolution spectroscopy of two different binary star systems, HIP 18532, also known as Epsilon Persei, and HIP 26736. The stellar spectrum of the stars can be used to determine the reduced mass of the binary system. Specifically, the shifts in the spectral lines can be used to determine the orbital period while Doppler shifts in light can be used to determine their orbital velocity. Additionally, the results of Epsilon Persei will corroborate new measurements of its orbital elements.

Acknowledgements

My deep gratitude to my thesis advisor, Ian Dell'Antonio, who guided me throughout my time in the physics department and my thesis. His excitement for astrophysics kept me engaged and inspired with my research. Above all, his kindness and generosity helped defined my time at Brown.

My appreciation extends to my colleagues at Community College Rhode Island, Brendan Britton and his teaching assistant, Zachary Sanborn. I am very grateful that Brendan agreed to let us use CCRI's observatory and spectrograph to observe spectroscopic binaries.

Thanks again to Ian and Brendan for providing me the opportunity, and supporting me, in conducting research in a manner that allowed me to be an amateur astronomy.

I would also like to thank my family and friends at Brown. Their perspective and encouragement has been incredibly helpful.

Chapter 1

Motivation

Studying close binary system's orbital dynamics provides insights into stellar evolution, to molecular cloud collapse, to cosmology of Type Ia supernovae and more. For my thesis, I measured the spectra of two known spectroscopic binary systems, HIP 18532 (further referred to as Epsilon Persei), and HIP26736, in order to detect their shift in the Hydrogen-alpha wavelength over the course of four weeks. Measurements of Sirius were also taken to be used as a control system. These measurements were taken using high resolution spectroscopic radial velocity monitoring. By measuring the Doppler shift in radial velocity, key aspects of the binary systems orbit were deduced. Observations of these spectroscopic binaries are significant for gaining a better understanding of how successful measurements of spectroscopic binaries can be in Providence Rhode Island using a 2400 lines/mm grating and stars visible in the winter/spring months. The results of which can be compared to current figures of three spectroscopic binary systems and relays how accurate our observations can be.

Epsilon Persei and HIP26736 were chosen in part because they are visible in the evening sky, have a apparent magnitude that is bright enough to observe consistently, and a a radial velocity that is significant enough to measure a shift. Epsilon Persei is located in the constellation of Perseus and has an apparent magnitude of 2.88. The right ascension of

Epsilon Persei is $03^h57^m51.23^s$ and its declination is $+40^\circ00'36.77"$. HIP26736 is in the constellation Orion and has an apparent magnitude of 4.95. The right ascension of HIP26736 is $05^h40^m50.72^s$ and its declination is $-01^\circ07'43.6"$. Recent observations of Persei's orbital period have showed conflicting results $14.06916^d \pm 0.00004$. Observations done in this thesis are compared to the results of "The new orbital elements and properties of ϵ Persei" (J.Libich).

1.1 Background

Binary stars systems are two stars that orbit a shared center of mass. These stars are gravitationally bound to each other but do not interact. Whereas visual binary star systems can be distinguished with a telescope or binoculars, spectroscopic binaries are too close together and/or too far away from Earth and they can only be distinguished by the Doppler shift in their spectrum. The stars are classified as 'A' for the primary brighter star and 'B' for the dimmer secondary star. In some cases, the spectral lines of both stars in the system are visible to the observer and the spectrograph will show spectral lines from both stars. This type of system is referred to as a double-lined spectroscopic binary (SB2)(J. Southworth).

William Herschel was the first to use the term *binary star* with his observation of stars that showed orbital motion. Hermann Karl Vogel was a German astronomer who discovered spectroscopic binaries (Britannica). The stars in these systems are close enough to each other, or are far enough away from the observer, that the stars are unable to be resolved by a telescope which differs from visual binaries. These binary systems are determined from the Doppler shifts in their spectral lines as the individual stars rotate around each other. If a star is moving away from the observer during its orbit, the wavelength of light will increase in length and be shifted to the red side of the spectrum, while if the star is moving closer to the observer, the wavelength of light will be compressed and shifted to the blue side of the

spectrum.

An important factor in the measurement of spectroscopic binaries is the orbital plane of the system. If the stars are in an orbital plane such that the the light emitted is at a right angle with the observer, then the observation will not detect any Doppler shift. If a system is at an inclination to the observer, the observed velocity is related to the orbital velocity by,

$$v_1 = \frac{v_{obs}}{sini} \tag{1.1}$$

where v_{obs} is the observed velocity and i is the angle of inclination. For binary systems were one star is more dominant over the other, the orbit, assuming it is near circular, can be calculated with the equation,

$$\frac{m_2^3}{(m_1 + m_2)^2} = \frac{Pv_1^3}{2\pi G} \tag{1.2}$$

Substituting in the orbital velocity, the new period is calculated with the equation,

$$\frac{m_2^3 sin^3 i}{(m_1 + m_2)^2} = \frac{Pv_{obs}^3}{2\pi G} \tag{1.3}$$

Other limiting factors are the components star's mass and distance from the primary star. Component stars with low mass, as well as, component stars that orbit distant from each other, will have a low velocities and reduce the chance of detection. Binaries with orbits that are within each others Roche limit can exchange material due to tidal interactions (J. Southworth).

There are several different configurations of binary stars systems. The first of which is a detached binary system. In these systems, each star is within its Roche lobe. The Roche lobe is the region surrounding the star within which material is gravitationally bound to itself and not the companion star. Most known binaries have this configuration.

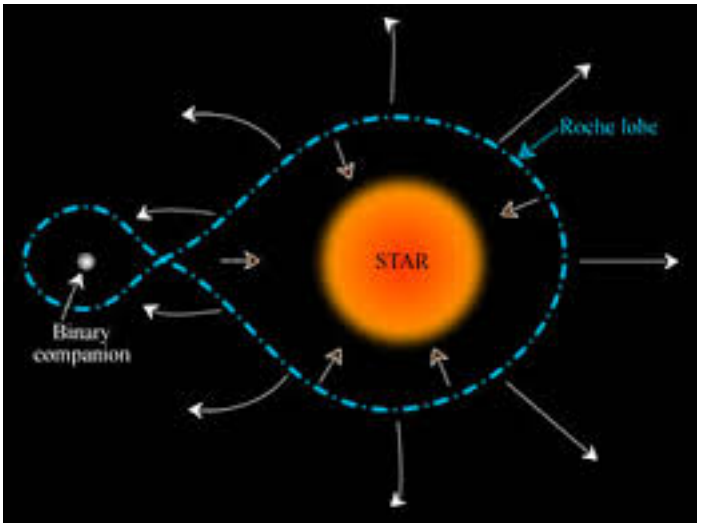

Figure 1.1: Roche lobe of star and binary companion

Another binary configuration is semidetached binary stars. These are systems in which one of the stars fills the binary star's Roche lobe while the other does not. If the companion object has a high gravitational pull, like a neutron star or a black hole, then the gas from the star can be pulled outwards to fill the lobe.

Lastly, contact binary are systems where both components of the binary fill their Roche lobes. The uppermost part of the stellar atmospheres forms a common envelope that surrounds both stars. As the friction of the envelope brakes the orbital motion, the stars may eventually merge.

In binary systems with a highly dense object like a white dwarf, neutron star, or black hole can accrete gas from their companion star. This releases gravitational potential energy in the form of thermal radiation. In other cases, if a star accrete's enough mass to reach the Chandrasekhar limit, the star will explode in a supernova.

The formation of binary stars is a natural consequence of star formation. Fragmentation of the molecular cloud during the formation of protostars is a possible explanation of the formation of a binary of multiple star system. It is also possible to have a three body system as well. In the case of Epsilon Persei, new research suggests that there is a third star in the system with a significantly larger orbit.

If the remaining system is free of significant perturbations, the two will form a binary. There is the case that gravitational capture between two stars could form a binary system but the likelihood is extremely low because of conservation of energy rules(Britannica).

1.1.1 Type of Measurement Needed to do this Project

Types of measurements needed to observe spectroscopic binaries involve a series of measuring specific spectral lines of the binary system at different times such that the shift in wavelength is noticeable. The spectra shifts are related to the radial velocity of one or both of the stars in the system. The radial velocity can be graphed as a function of time and, as such, produce a graph of the orbital phase.

Measurements of spectra in the $6400 - 6600$ Angstrom range were chosen in order to observe the H-alpha line of the binary stars. The H-alpha line is useful because it has a prominent absorption line. In the conditions of an Earth based spectrograph combating atmospheric influence and light pollution, the H-alpha line is strong enough to be observed. We have to take multiple spectra's on a given night which is then averaged together to help rid of any fluctuations or errors in a single spectrum. The spectra are compared over each observing session to see the shift in wavelength. In converting the shift in wavelength to velocity, an adjustment was made to account for the movement of Earth around the Sun, making the velocity a heliocentric velocity.

1.1.2 Hydrogen Alpha Line

In the observations of Sirius, Epsilon Persei, and HIP 23676, the spectrograph gratings were set to be centered on the Hydrogen Alpha line. Hydrogen Alpha, also referred to as H-alpha, line is a spectral line in the Balmer series where an electron falls from the third energy level to the second energy level. H-alpha spectral line has a wavelength of 656.281nm. The line falls in the visible red part of the electromagnetic spectrum. Astronomers use the H-alpha line to trace ionized hydrogen content of gas clouds in space. The H-alpha line is easily

saturated because hydrogen is the dominant element of nebulae, indicating the shape and boundaries of the cloud but not the mass.

Hydrogen is one of the most abundant elements in stars, especially in main sequence stars where hydrogen is fused to make helium and other elements. In the outer layers of the star, the photosphere and the chromosphere, the temperature is cool enough such that atomic hydrogen exists. In the chromosphere, temperature rises from $11,000^{\cdot}F$ to $36,000^{\cdot}F$ In these layers are were hydrogen absorption and emission spectra can be observed (Cram Mullan).

1.1.3 Doppler Shift

The Doppler shift is a change in frequency of a wave in relation to the observer who is moving relative to the wave source. If a source is approaching the observer, the frequency of the wave is compacted because each successive wave emitted is for a position closer to the observer than the previous. The time between each emitted wave is shorter, increasing the frequency and therefore the waves compress together. The increased frequency corresponds to a blue shift in the electromagnetic spectrum. Inversely, the same is true for a receding object, increase in time, a reduction in frequency, and a redshift in spectrum.

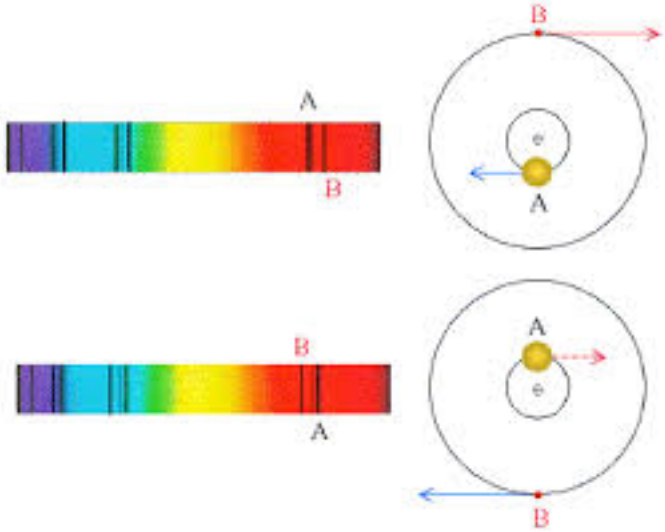

Figure 1.2: Caption

Doppler broadening is the broadening of spectral lines caused by the Doppler effect resulting from a distribution of velocities of atoms or molecules. The different velocities of the emitting particles result in different Doppler shifts which cumulate to the line broadening.

For example, atoms in a gas at temperature T have a velocity,

$$v_0 = \sqrt{\frac{2kT}{m}} \tag{1.4}$$

Although heavier atoms move slower and since not all atoms move at the same speed, the velocities can be described as a Maxwellian distribution,

$$f(v)dv = \frac{1}{\sqrt{\pi}} e^{-(v^2/v_0^2}dv/v_0 \tag{1.5}$$

With this distribution, one can obtain an effective absorption coefficient using linear Doppler effect at all velocities,

$$\alpha_{eff}(\nu) = \int_{-\infty}^{\infty} \alpha(\nu(1 - v/c))f(v)dv \tag{1.6}$$

The linear Doppler effect at all velocities is valid because α falls of quickly with frequency, ν.

Plugging the Maxwellian distribution, $f(v)$ into the absorption coefficient equation and integrating results in,

$$\alpha_{eff}(\nu) = \frac{\sqrt{\pi e^2}}{m_e c} f_{lu} \frac{H(a, \nu}{\Delta\nu_D} \tag{1.7}$$

Where $\Delta v_D = v_0/c$, $y = v/v_0$ and $a = \Gamma/(4\pi\Delta v_D)$. Here $H(a, \nu)$ is the Voigt function defined as,

$$H(a, \nu) = \frac{a}{\pi} \int_{-\infty}^{\infty} \frac{e^{-y^2}}{((v - y)^2 + a^2)} dy \tag{1.8}$$

which describes the spectrum from a star. The Voigt function has a Gaussian core (from

velocities), and Lorentian tails.

(From class notes) bound-bound transition there is finite lifetime of the energy level that leads to an absorption coefficient Lorentzian profile,

$$\Phi(\nu) = \frac{\Gamma}{4\pi^2}(\frac{1}{(\nu - \nu_0)^2 + \frac{\Gamma^2}{4\pi}} \tag{1.9}$$

Where Γ is the natural width of the line. The natural width is the sum of the spontaneous emission Einstein coefficients that correspond to transitions down from both the two states in consideration.

Transitions from state i to j, the natural width is

$$\Gamma_{ij} = \sum_{k<j} A_{jk} + \sum_{k<i} A_{ik} \tag{1.10}$$

For example, the lifetime of the H-alpha line of hydrogen, which is a 3-2 transitions is,

$$\Gamma_{32} + A_{31} + A_{21} \tag{1.11}$$

This would work if the atoms were lonesome and not in a gas. In a gas, the atoms collide causing energy level transitions with no photon emission. The energy instead becomes kinetic energy of the gas. If the energy rate at which collisions change the state is v, and then the natural width becomes $\Gamma_{eff} = \Gamma + 2v$ (Dell'Antonio).

1.1.4 Reduced Mass Calculation in Binary Stars

Binary star systems are a vital way for scientists to determine the mass of a star. The gravitational pull of one star on another causes them to orbit around a shared center of mass. The combined masses of the system is given,

$$P^2 = \frac{4\pi^2}{G(m_1 + m_2)} r^3 \tag{1.12}$$

Where P is the orbital period of the system, r is the separation distance between two stars whose masses are m_1 and m_2.

To calculate the center of mass in a simple binary system,

$$r_1 = a \cdot \frac{m_2}{m_1 + m_2} \tag{1.13}$$

where a is the distance between the two stellar centers and m_1 and m_2 are the masses of each star.

To determine the radial velocity, measurements of the wavelength of the Hydrogen alpha spectrum was obtained. The difference between the known wavelength of Hydrogen Alpha, $6,562.80$ Angstroms, and the observed wavelength. The ratio of the change in wavelength over the known wavelength relates to the radial velocity via,

$$\frac{\Delta\lambda}{\lambda_0} = \frac{\Delta v}{c} \tag{1.14}$$

where λ_0 is the rest wavelength of the spectral line, c is the speed of light, and Δv is the change in velocity (J. Southworth).

In order to calculate the velocity curve from the elements of a binary, it is useful to visualize the system as a plane tangent to the celestial sphere.

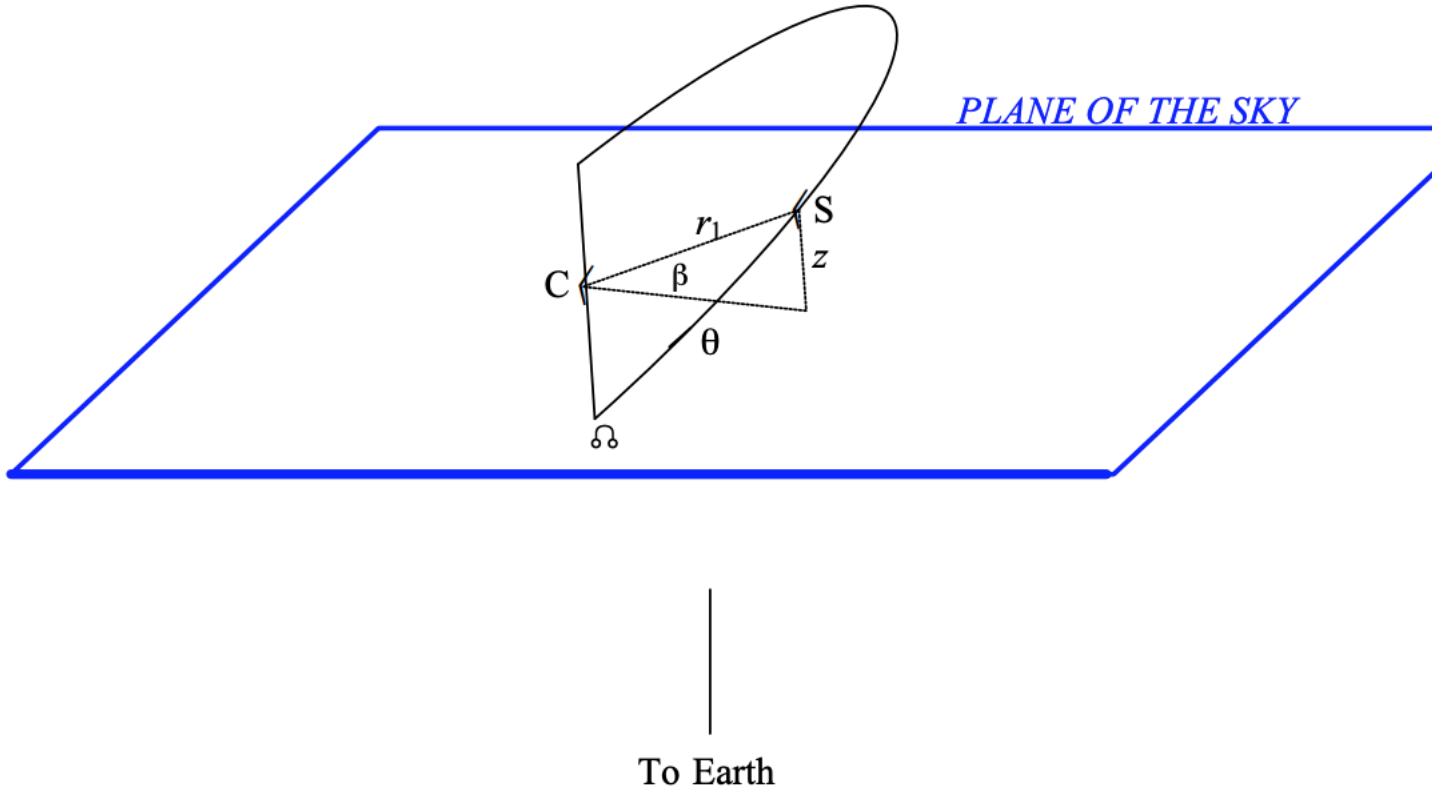

Figure 1.3: Star 1, S, in orbit around C. The argument of latitude of S is θ, and its distance from C is r_1. The stars distance above the plane of the sky is z, and $z = r_1 sin\beta$. The inclination of the plane of the orbit to the plane of the sky is i

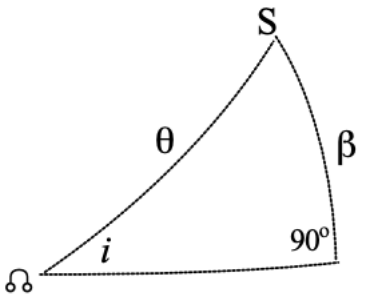

Figure 1.4: The angles on the surface of the sphere where the sphere is centered at C and is of some arbitrary radius

The modified equation for the triangle is, $sin\beta = sinisin\theta$. Where θ is the argument of latitude, $\theta = \omega + v$ where ω is the argument of periastron and v is the true anomaly.

$$z = r_1 sin(i) sin(\omega + v) \tag{1.15}$$

The radial velocity, V, of star 1, S, relative to the Sun is,

$$V = V_0 + \dot{z} \tag{1.16}$$

Where V_0 is the radial velocity of the center of mass C (also referred to as the systemic velocity).

Differentiating equation of angular momentum per unit mass, $r_1^2\dot{v} = na_1^2\sqrt{1-e^2}$ where a_1 is the semi major axis of star 1 about C and n is the mean motion, $2\pi/P$ with respect to time provides,

$$\dot{z} = sin(i)[\dot{r}_1 sin(\omega + v) + r_1\dot{v}cos(\omega + v)] \tag{1.17}$$

Expressing this equation in terms of the true anomaly v instead of v and r_1. The equation of the ellipse is then,

$$r_1 = \frac{l_1}{1 = ecos(v)} = \frac{a_1(l - e^2)}{1 + ecos(v)} \tag{1.18}$$

where l_1 is te semi latus rectum, $l_1 = a_1(1 - e^2)$. Taking the first derivative of the equation of the ellipse is,

$$\dot{r}_1 = \frac{l_1 e\dot{v}sin(v)}{(1 + ecos(v)^2} = \frac{r_1 e\dot{v}sin(v)}{1 + ecos(v)} \tag{1.19}$$

Combining this with equation 1.21,

$$\frac{\dot{z}}{sin(i)} = r_1\dot{v}(\frac{esin(v)sin(\omega + v)}{1 + ecos(v)} + cos(\omega + v)) \tag{1.20}$$

Simplifying with equation 1.22 and the angular momentum per unit mass,

$$\frac{\dot{z}}{sin(i)} = \frac{na_1}{\sqrt{1-e^2}}(esin(v)sin(\omega+v) + (1+ecos(v)cos(\omega+v)) \tag{1.21}$$

Knowing that $esin(v)sin(\omega+v) + ecos(v)cos(\omega+v) = ecos(\omega)$, the result is,

$$\dot{z} = \frac{na_1 sin(i)}{\sqrt{1-e^2}(cos(\omega+v) + ecos(\omega} \tag{1.22}$$

K_1 being the semi-amplitude of the radial velocity curve. K_1 is defined as,

$$K_1 = \frac{na_1 sini}{\sqrt{1-e^2}} \tag{1.23}$$

Finally, the radial velocity curve equation, as a function of the true anomaly and the elements is

$$V = V_0 + K_1(cos(\omega+v) + ecos\omega) \tag{1.24}$$

where $v = v(t, T, e)$. The true anomaly is found first from the mean anomaly equations,

$$M(t) = \frac{2\pi}{P}(t-\tau) \tag{1.25}$$

also known as the Kepler's equation,

$$M(t)) = E(t) - esin(E(t)) \tag{1.26}$$

where E(t) is the eccentric anomaly. Given that its a transcendental equation the Newton-Raphson method is able to solve the taylor expansion of the equation using,

$$tan\frac{E(t)}{2} = (\frac{1+e}{1-e})^{-\frac{1}{2}} tan(\frac{v(t)}{2}) \tag{1.27}$$

From the radial velocity curve, one can determine V_0, K_1, e, ω and T. The subscript 1

refers to a single lined binary of the observable star and the subscript 2 refers to the secondary star. The radial velocity varied between a maximum of $V_{max} = V_0 + K_1(ecos\omega + 1)$ and a minimum of $V_{min} = V_0 + K_1(ecos\omega - 1)$. The difference between the min and max is $2K_1$. The mean motion, n was determined to to be $\frac{2\pi}{P}$. Rearranging n to solve for P, and knowing e and K_1, then one can solve for $a_1 sini$.

$$n^2 a_1^3 = GM \tag{1.28}$$

where

$$M = \frac{m_2^3}{(m_1 + m_2)^3} \tag{1.29}$$

Combining equation 1.29 and 1.30 gives,

$$K_1 = \frac{G}{(1 - e^2)a)1sini} x \frac{m_2^3 sin^3 i}{(m_1 + m_2)^2} \tag{1.30}$$

thus the mass function, $\frac{m_2^3 sin^3 i}{(m_1+m_2)^2}$ can be determined (University of Victoria).

1.2 Instrument

The Lhires III was the spectrograph used for these observations with a 2400mm grating. Lhires is an acronym for Littrow HIgh REsolution Spectrograph. The spectrograph is optimized for high-resolution spectroscopy and was used on a 16 inch telescope. The spectrographs $200mm$ lens act as both the collimator to render the light beam parallel, and the focusing lens to bring a focused image of the spectrum onto the detector. The spectrograph has the resolving power,

$$\frac{\lambda}{\Delta\lambda} \tag{1.31}$$

, around $17,000$ in the red which correlates to a resolving spectral details smaller than 0.4 angstroms.

Figure 1.5: Shelyak LHIRES III

The spectrograph contains a neon calibration lamp. A reference spectrum was taken with the neon lamp after the exposures of the spectrum of the binary stars. For example, if multiple exposures were taken on the same star, then one neon spectrum was taken after the last exposure. The reason for the reference spectrum is because the spectrograph is

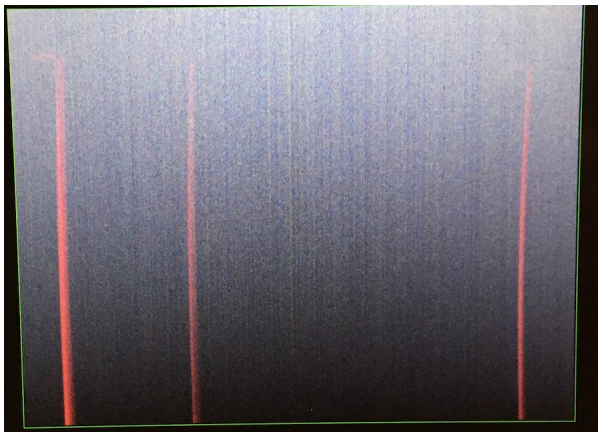

Figure 1.6: Neon exposure

not stable over temperature and flexion. The reference star will be used to calculate the

response curve of the full setup. Bias, dark, and flat field frames can also be used to correct images from these defects and were partially used in the observations. During one observing night dark frames were taken with each star but the dark current was found to be too small to significantly affect the spectra. Other features of the spectrograph include a micrometer to set the wavelength of observations. For the binary stars observed, the spectral range of $6500 - 6700$ Angstroms was used. Other aspects of the spectrograph include a guiding hole which connected with a camera to guide the scope to the correct star. Furthermore there was the ability to adjust the mirror slit and to focus the doublet. The entrance slit to the spectrograph is highly polished and reflective with a 10° incline to the optical axis of the telescope. Light from the polished surface is reflected back to the guide camera via a $1\frac{1}{4}$ inch adapter ring.

The spectrograph itself has a fixed mirror slit. This slit can be removed and the width can be adjusted as well. The focused light from the telescope passing through the slit hits a 45° mirror, sent to the collimator lens, which is then passed to the plane reflection grating that is mounted on a pivoting support. By adjusting the rotation of the grating via a micrometer screw, we were able to achieve the spectral range of the spectrograph that we wanted.

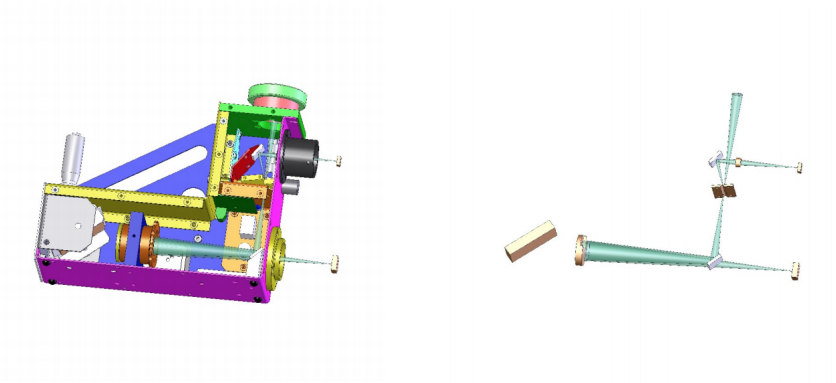

Figure 1.7: Internal Mechanisms of LHIRES III

One of the methods we used to focus the guiding camera on the subject was place a slitted sheet of metal over the 16inch telescope which would scatter light from the star if the star was not in perfect focus. Using the diffraction as a guide, we were able to tune the

focus to be perfectly on the star. The dispersed light from the grating passes back through the lens and is focused on the detector, which was a CCD camera (Shelyak).

Chapter 2

Process

The previous section described the spectrograph, LHIRES III, and how it was set up for this experiment. Once the spectrograph was attached to the 16inch telescope, the guiding system slewed to Sirius which was used as our reference star. From here, we would make micro adjustments to the position of the telescope to get Sirius directly into the slit of the spectrograph. We also adjusted the focus on each star in order to obtain the best precision and reduce light noise.

After the Star was positioned to our satisfaction, exposures of Sirius were made ranging from 10sec to 15sec. This was an adequate amount of time to observe Sirius because of its high apparent magnitude. Each observing session had at least three exposures of Sirius. Following the exposure, a reference spectrum of the Neon lamp was taken, again for 10 seconds. On the guiding software, we would calibrate the pointing to the position of Sirius and then slew to Epsilon Persei. Calibrating on Sirius would provide a more accurate model of the telescope pointing, allowing easier acquisition of the faint stars.

The initial exposures of Epsilon Persei were for one minute but that short of time produced a very noisy spectra so the subsequent exposures were 240 seconds (four minutes), and three exposures per night. For HIP26736, because it is the faintest star observed, exposures of 240 seconds were also used with three exposures for the first few observation sessions,

and five exposures for the last observation session. Taking more exposures brought greater definition to the H-alpha line and reduced noise.

2.1 IRAF

The raw spectra exposures were processed using the astronomy software IRAF. In the spectra, the peak wavelength, H-alpha, was first identified and the background was fitted. The Neon lines were identified and used as a reference to its correlating star. The Neon lines used were 6506, 6532, and 6598. The wavelength scale was calibrated by fitting Chebychev polynomials up to order 5, although no polynomial was fitted past order 1. The calibrated spectra were then cleaned of cosmic rays and any other fluctuations. Using a Gaussian fit, the wavelength of H-alpha and telluric lines (6516.5 Angstroms and 6543.9 Angstroms) in Earth's atmosphere were found. The telluric lines are used as controls since they are constant in Earth's atmosphere. If there was a shift in the telluric line, that difference was adjusted for in the H-alpha line. Specifically, the difference in telluric line 1 and telluric line 2 were found and the average of those differences was calculated. That average difference was then subtracted from the H-alpha line to account for any errors in the neon calibration.

When all of the spectra of a star for a particular night were identified and cleaned, the final exposures were then combined on IRAF using scombine function with the weight set to median. Again, the final summed spectra was cleaned of cosmic rays and hot pixels and a Gaussian curve was fitted to find the wavelength of H-alpha.

The wavelength of H-alpha corresponds to velocity via equation 1.18. This velocity, however, is the velocity of the binary star around its orbit as us, the observer, orbits the Sun. Earth's radial velocity is significant enough that the the velocities observed were converted into a heliocentric velocity. This process was done using IRAF's rvcorrect task. An text file was created per star, containing the year, month, day, universal time, right ascension, and declination. The observatory function was utilized to identify our exact right ascension,

declination, and altitude. Rvcorrect can then calculate the heliocentric radial velocity in km/s. The observed velocity is corrected for the rotation of the Earth, the motion of the Earth about the Earth-Moon barycenter, and the orbit of the barycenter about the Sun (IRAF rvcorrect).

```
cl> noao
cl> onedspec
cl> twodspec
cl> apextract  cl> apall science_exposure_filename

cl> apall science_exposure_filename2 ref=science_exposure_filename

cl> hedit science_exposure_filename.ms REFSPEC1 "cal_lamp_exposure_filename" add+
cl> dispcor science-exposure-filename calibrated-science-exposure-filename

Lines ('f'ile, 'g'aussian, 'l'orentzian, 'v'oigt, 't'ype, 'q'uit:

     cl> rvcorrect
```

```
cl> type rv.obs
1987 10 21 11:00:24  3:36:15   0:22:04
1987 10 21 11:08:00  8:19:35  -0:51:35
1987 10 21 11:15:47  8:35:12   6:40:29
1987 10 21 12:12:10  9:13:20  61:28:49
1987 10 21 12:16:03  9:27:48   9:07:08
1987 10 21 12:20:43  9:50:45  -6:06:58
1979  3 25 11:22:59 16:07:28 -23:37:49 0 -67.5
cl> rvcorrect f=rv.obs > rv.dat
cl> type rv.dat
##    HJD          VOBS   VHELIO     VLSR   VDIURNAL   VLUNAR  VANNUAL   VSOLAR
2447089.96358     0.00    11.07    -2.74     -0.189    0.008   11.246  -13.808
2447089.96296     0.00    28.05    13.56      0.253    0.010   27.790  -14.498
2447089.96813     0.00    29.04    16.64      0.262    0.011   28.770  -12.401
2447090.00834     0.00    22.06    25.26      0.114    0.010   21.940    3.200
2447090.00884     0.00    27.70    18.55      0.250    0.009   27.438   -9.152
2447090.01129     0.00    23.99    13.50      0.275    0.007   23.704  -10.484
2443957.97716   -67.50   -41.37   -31.48      0.002    0.012   26.117    9.884
```

Figure 2.1: IRAF steps for Spectra Analysis and Heliocentric velocity

2.2 Epsilon Persei

Epsilon Persei (ϵ Per) or HIP 18532, is a multiple star system located in the northern part of the constellation Perseus. Originally thought to be a binary star system, new studies have found evidence that there is a third star in the system (J. Libich.). The third star has a significantly longer period than the main two stars which have a period of 14.06916 days. Epsilon Persei has an apparent magnitude of 2.88 making it bright enough to see

with the naked eye in the night sky. The spectral class of ϵ Per is B0.5 III (Morgan et al. 1943) although it is also classified as B0.5V (Johnson Morgan 1953). Epsilon Persei is located about 640 ± 30 light years from Earth) with a parallax of 5.11 ± 0.23 . Other orbital elements of ϵ Per are the epoch of periastron is 47767.543 ± 0.024, the argument of periastron is argument of periastron ω: $105.8 \pm 1.2°$, the semi-amplitude (K_1): 15.23 ± 0.20 km/s, and lastly the eccentricity is 0.5549 (Whitworth, N.).

New studies on the spectral observations of Epsilon Persei confirm that there is a periodic variation of the systemic velocity. Together with new evidence from astrometric observations, they confirm the existence of a third body in the system with an orbital period of about 9600 days (26.3 years), rather than the previous measurement of 4156 days (J. Libich)

2.3 HIP 26736

HIP 26736 binary system is in the constellation Orion. It has a right ascension of $05^h40^m50.72^s$ and declination of $-01°07'43.6"$. HIP 26736 has a spectral type of B3V and an apparent magnitude 4.95. HIP 26736 is located about 900 light years from Earth and has a parallax of 3.63 ± 0.37. The period is 27.1546 days. Other orbital elements of HIP 26736 are, semi-major axis is 8677, the semi-amplitude (K_1) is 57.9 km/s, the argument of periastron (ω), is 78 and the eccentricity is 0.72(N. Kameswara).

Chapter 3

Results

The results of these observations discuss the analyzed data from our observations compared to the established orbital elements. Beginning with the control star, Sirius, below is a cleaned spectra from Sunday, February 23rd. Sirius has a deep absorption feature at the H-alpha line and two smaller water vapor absorption feature s at 6516.5 Angstroms and 6543.9 Angstroms.

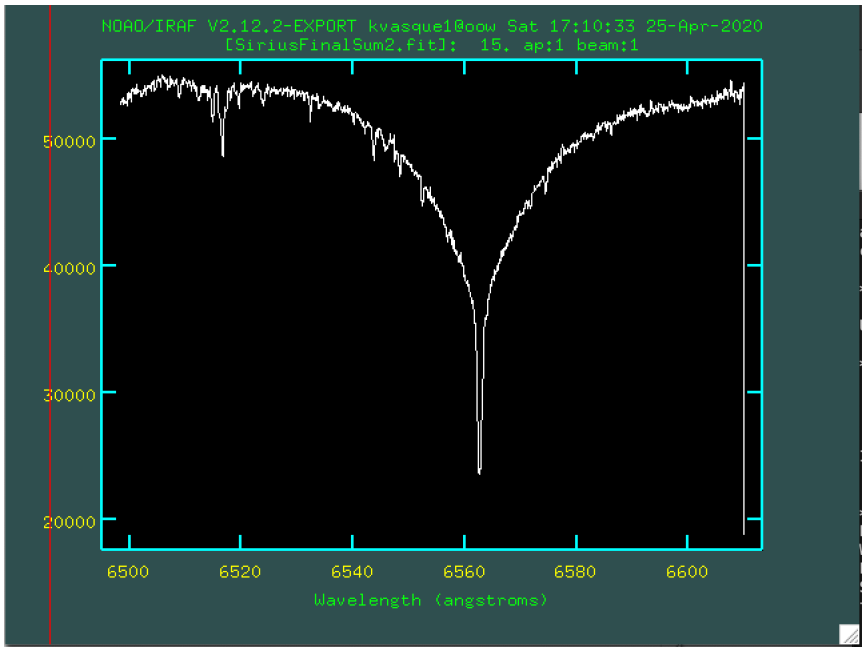

Figure 3.1: Sirius spectra on February 23rd 2020

Comparing the calculated observed velocity versus the theoretical is shown below,

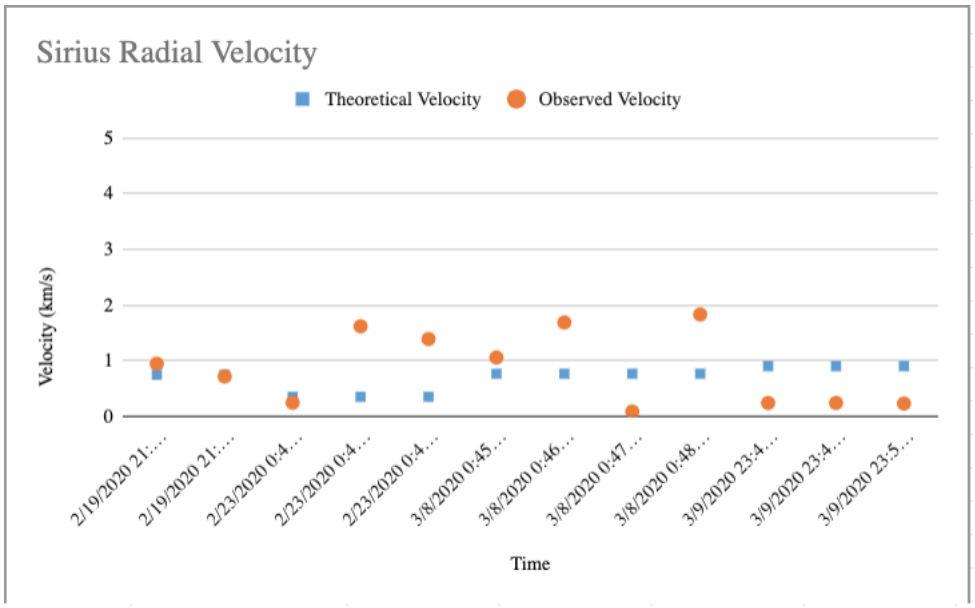

Figure 3.2: Sirius Observed Radial Velocity vs the Expected Velocity

The graph shows the radial velocity at each observation date. The fluctuations in velocity vary between 0 km/s and 2 km/s.

Next is Epsilon Persei. Below shows a spectra taken on Sunday, March 8th. Again there

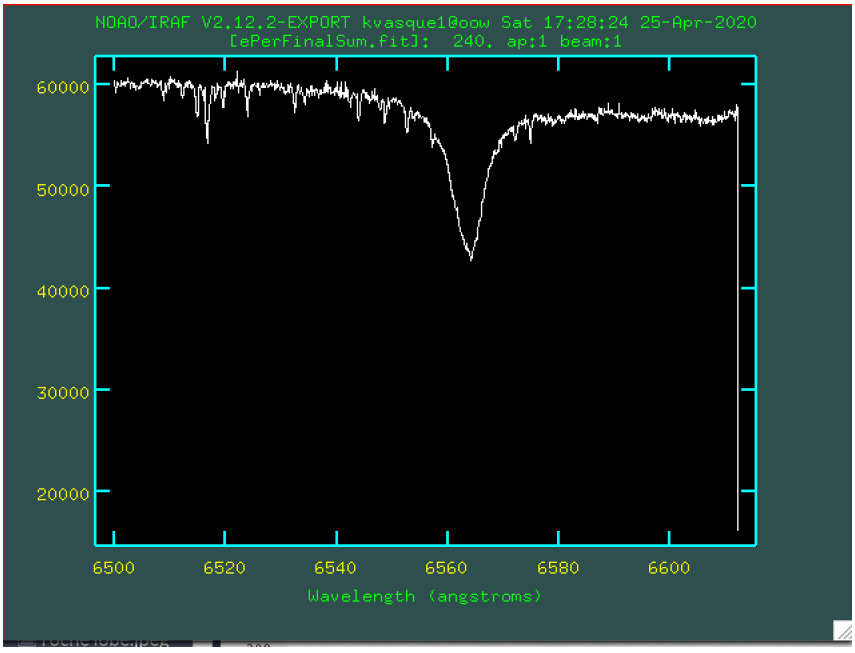

Figure 3.3: Epsilon Persei on March 8th

is a steep absorption feature at the H-alpha line and visible water vapor lines at 6516.5 Angstroms and 6543.9 Angstroms. The width of ϵPer is wider at this date compared to, Given that the absorption feature is shifting to a larger value, this corresponds to when ϵPer

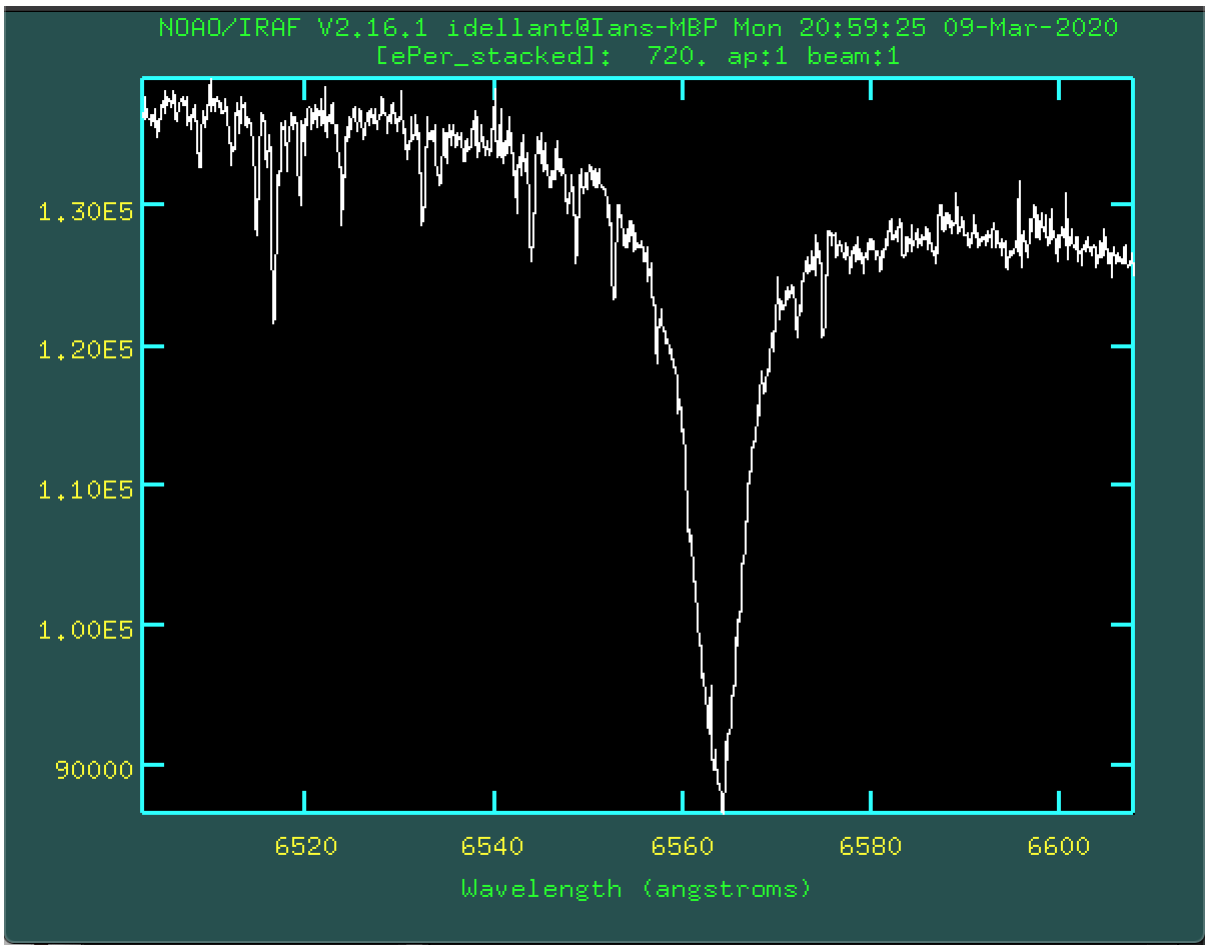

Figure 3.4: Epsilon Persei on March 9th

is receding from Earth. The absorption features on the left of the H-alpha line are the telluric lines from Earth's atmosphere. March 9th was a humid and cloudy day which increased the intensity of these absorption features. Comparing the calculated observed velocity versus the theoretical is,

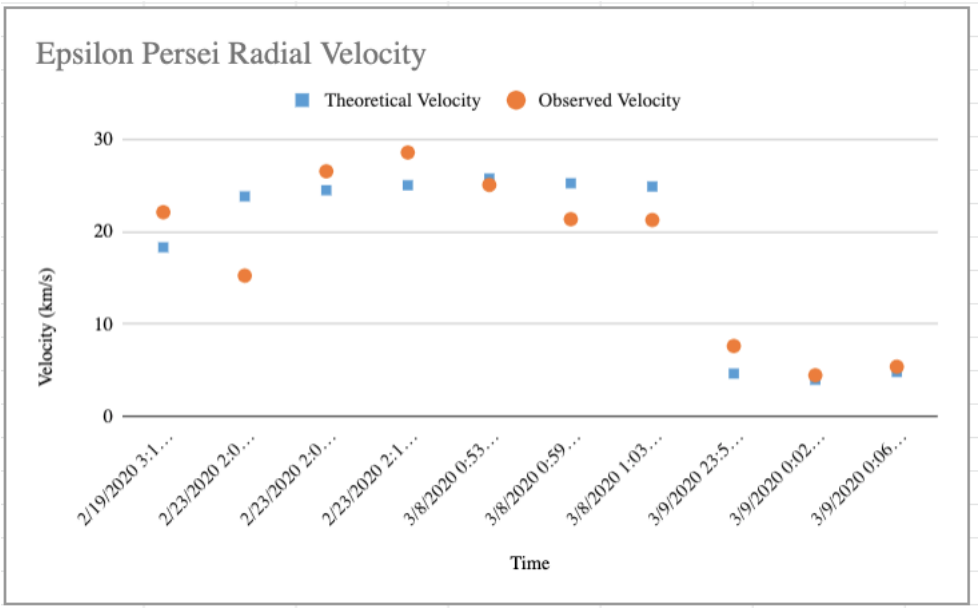

Figure 3.5: Epsilon Persei Observed Radial Velocity vs the Expected Velocity

It is important to note that the dates, 2/23/2020 and 3/8/2020 are exactly two weeks apart which aligns with the 14 day period of ϵPer. This means that the graph appears constant for half the dates. In reality, due to ϵPer high eccentricity, the radial velocity curve looks more like,

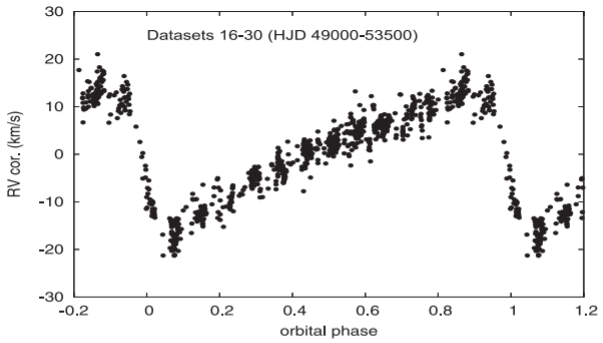

Fig. 1. *From top to bottom*: the RV curves (corrected by γ velocity) phased according to orbital period $14^{d}.06915$ and the elements from solution 4 for all data and for the datasets sorted by time from the oldest datasets to the newest datasets (see Table 4).

Figure 3.6: ϵPer Radial Velocity Curve: J. Librch

Finally, the results HIP 26736. Below is a spectra of HIP 26736 that has been combined and weighted of all of the exposures from March 8th to show the absorption feature.

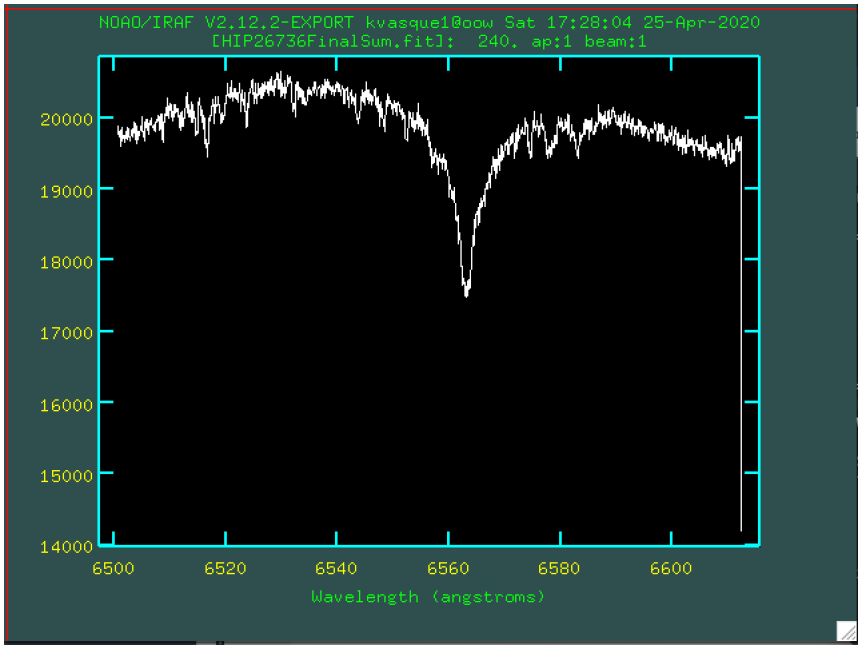

Figure 3.7: HIP26736 on March 8th

HIP 26736 has a very high eccentricity (0.72). As a result the expected radial velocity curve, shown below, has steep drops and slow rises.

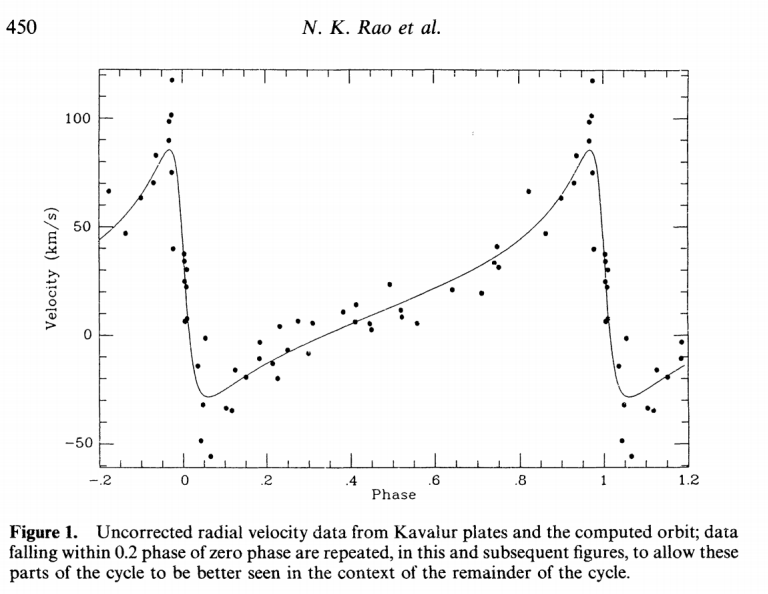

Figure 1. Uncorrected radial velocity data from Kavalur plates and the computed orbit; data falling within 0.2 phase of zero phase are repeated, in this and subsequent figures, to allow these parts of the cycle to be better seen in the context of the remainder of the cycle.

Figure 3.8: Radial Velocity Curve of HIP 26737 with varying systemic velocity factor, Roa, Kameswara

Chapter 4

Conclusion

In this project, observations of spectroscopic binary star systems were taken over six observation sessions. Due to the quality of the exposures and adjustments of binaries themselves, three to four of those observation sessions were utilized. From those exposures, the data was cleaned, fitted, and combined to increase the quality of data. The hydrogen alpha line, 6562.8 Angstroms, was the reference point to compare the Doppler shift of the binary star. In IRAF software, a Gaussian fit was used to find the peak wavelength of the absorption lines. Water vapor absorption lines in Earth's atmosphere were used to correct fluctuations in the H-alpha line in the spectra. Using equation 1.18, the velocity of the binary star was calculated. The heliocentric velocity of Earth, the observer, at each observation session was then subtracted from the observed velocity to obtain a true velocity of the binary star.

The expected radial velocities of the binary systems where calculated using equation 1.28. Known values for the semi-amplitude, K_1, argument of periastron ω, the semi major axis a_1, period, P, and eccentricity. Solving the Kepler equation, 1.30, for the mean anomaly provided the information needed to solve for the true anomaly, which is a function of time.

For the control star, Sirius, observations were in line of the expected value. The velocities were between $0 - 2$ km/s which is fairly steady but also provides the limits to which observations in Rhode Island using a 2400lines/mm grating spectrograph. Because Sirius is

a binary star with a period of about 50 years, the radial velocity of Sirius shouldn't change in the course of six weeks.

Fortunately, for both ϵPer and HIP26736, the results were able to match the predicted velocity to some degree and the phase of the star system. For ϵPer, one data point on 2/23/2020 was lower than the rest of the other data points in that session which and the data points from 3/8/2020 are sloping down/ at a lower velocity than observed. The radial velocity curve had an amplitude up to 30km/s which corroborate well with new observations of ϵPer, however there aren't enough data points to conclusively say that the full radial curve matches the variations in the systemic velocity found in the study (J. Libich).

Some potentially reasons for error are from focusing the star on the slit during observations. The star will drift off the focus of the telescope as the Earth rotates. Focusing the slit perfectly, and keeping the star in focus over the four minute exposures (adjusting at the rate the Earth is rotating), was a challenge. We had to manually move the telescope throughout the duration of the exposure to keep the star in focus. Attempts at using a guiding camera on the telescope to follow the star as Earth rotates wasn't successful because most of the light from the star went into the slit and was not reflected back, which is what the guide camera would have focused on. The guide camera looks at the whole field of view. If the companion star was visible, the guide camera could have focused on it, but with spectroscopic binaries the companion star isn't visible in a telescope. Consequently, this may have decreased the intensity of the peak and increased the spread of the absorption feature. A wider H-alpha absorption feature makes it more difficult to determine the center and obtain an accurate value. This error is likely the source of varying velocity.

HIP 26736 had similar issues in addition to it being a dimmer star. The dimness contributes to the amplitude of the velocity curve and the results showed an error of ± 5 km/s. While the data points are more constant across, there is more variation in the speed. For the observation dates on 2/19/2020, the observation times and number of observations were lower. For example, during the first observation session three, 60 second exposures were

taken which concluded in nosier spectra with more error. On 2/23/2020 three, 240 second exposures were taken which provided better data, but still enough noise that the quality could be better. On March 8th, five 240 second exposures were taken and this provided the best, most precise and accurate data.

In an ideal world, I would have been able to take more observations of each star. One of the fun challenges of this project was learning how to use the LHIRES III spectrograph for the first time alongside our colleges at CCRI. This did mean that the first time or two using the spectrograph had some trial and errors and was an adjustment period. A second challenge was finding a proper binary system that was observable in the Northern hemisphere in winter time and was bright enough to be observed. We attempted five to six different star systems before settling on Epsilon Persei and HIP 26736 as viable binary star systems. On a less fun note, the cancellation of school and social distancing per Covid-19 prevented me from obtaining more observations. Additional data points would have provided a more complete velocity curve and precise radial velocities.

Nonetheless, I am very grateful to have been able to complete a thesis on a project that has allowed me to be an amateur astronomer, improve upon my telescope skills, and work alongside some brilliant astrophysicists.

Figure 4.1: The good ol days

Chapter 5

References

- Abt, Helmut A., et al. "Rotational Velocities of B Stars." The Astrophysical Journal, vol. 573, no. 1, 2002, pp. 359–365., doi:10.1086/340590.

- Beauge, C., et al. "Planetary Masses and Orbital Parameters from Radial Velocity Measurements." Gehirnamp;Geist, 2007, www.gehirn-und-geist.de/sixcms/media.php/370/Leseprob

- Cram, L.E., and D.J. Mullan. "Formation of the Ha Absorption Line in Chromospheres of Cool Stars." 1985ApJ...294..626C Page 633, 30 Nov. 1984, articles.adsabs.harvard.edu/cgi-bin/nph-iarticle$_{q}uery?bibcode = 1985ApJ...294..626Camp; db_{k}ey = ASTamp; page_{i}nd = 7amp; plate_{s}elect = NOamp; data_{t}ype = GIFamp; type = SCREEN_{G}IFamp; classic = YES.$

- Czekala, Ian, et al. "DISENTANGLING TIME SERIES SPECTRA WITH GAUSSIAN PROCESSES: APPLICATIONS TO RADIAL VELOCITY ANALYSIS." Arxiv.org, Astrophysical Journal, 21 Feb. 2017, arxiv.org/pdf/1702.05652.pdf.

- Dell'Antonio "Doppler Broadening" Physics 1250 Stellar Structure, Brown University, 30 Mar. 2020

- The Editors of Encyclopaedia Britannica. "Hermann Karl Vogel." Encyclopædia Britannica,

Encyclopædia Britannica, Inc., 30 Mar. 2020, www.britannica.com/biography/Hermann-Karl-Vogelref207187.

- Giesen, Juergen. "Solving Kepler's Equation of Elliptical Motion." Solving Kepler's Equation, 5 Jan. 2016, www.jgiesen.de/kepler/kepler.html.
- "HD 37756." Wikipedia, Wikimedia Foundation, 11 Apr. 2020, en.wikipedia.org/wiki/HD$_3$7756$cite_note-Kameswara1990-10$.
- Libich, J., et al. "The New Orbital Elements and Properties of ϑ Persei." Astronomy amp; Astrophysics, vol. 446, no. 2, 2006, pp. 583–589., doi:10.1051/0004-6361:20053032.
- Murray, Carl D, and Alexandre C.M. Correia. "Keplerian Orbits and Dynamics of Exoplanets." Arxiv.org, 25 Feb. 2011, arxiv.org/pdf/1009.1738.pdf.
- Rao, Kameswara, et al. "The Eccentric Double-Lined Binary BD -1 1004." NASA/ADS, Astrophysical Journal, Dec. 1990, ui.adsabs.harvard.edu/abs/1990JApA...11..445K/abstract.
- "RVCORRECT." Iraf.net, Nov. 1990, iraf.net/irafhelp.php?val=rvcorrectamp;help=Help
- Southworth1, J. "BINARY STARS: A CHEAT SHEET." Arxiv.org, 7 Jan. 2020, arxiv.org/pdf/1912.13400.
- "Spectroscopic Binary Stars." University of Victoria, 2018, astrowww.phys.uvic.ca/ tatum/celmechs/celm18.pdf.
- Stevens. "33.3 Heliocentric Radial Velocity Calculation." Stsci, 1997, www.stsci.edu/documents/dhb/webv
- Whitworth, N. "Epsilon Persei (45 Persei) Star Facts." Universe Guide, Universe Guide, 24 Aug. 2019, www.universeguide.com/star/18532/epsilonpersei.

Appendix A

Data Tables

A.1 Tables

Sirius Results Table

Date	Observed Velocity	EPOCH Time	Mean Anomaly	Deg	True Anomaly	Theoretical Velocity
2/19/2020 21:47:00	0.9508	1582166820	6.288233628	360.2892474	1.39709	0.7543205346
2/19/2020 21:47:00	0.7222	1582166820	6.288233628	360.2892474	1.39709	0.7543205346
2/23/2020 0:45:32	0.2520	1582436732	6.289306378	360.3507115	1.69393	0.3580543482
2/23/2020 0:46:15	1.6233	1582436775	6.289306549	360.3507213	1.69397	0.358046852
2/23/2020 0:47:02	1.3948	1582436822	6.289306735	360.350732	1.69403	0.3580356101
3/8/2020 0:45:38	1.0639	1583646338	6.294113889	360.6261616	3.02385	0.7717118768
3/8/2020 0:46:35	1.6925	1583646395	6.294114116	360.6261746	3.02392	0.7717619269
3/8/2020 0:47:15	0.0926	1583646431	6.294114259	360.6261828	3.02396	0.7717905277
3/8/2020 0:48:11	1.8353	1583646491	6.294114497	360.6261965	3.02402	0.7718334301
3/9/2020 23:48:58	0.2467	1583812138	6.294772852	360.6639174	3.20609	0.9073955388
3/9/2020 23:49:56	0.2467	1583812196	6.294773082	360.6639306	3.20615	0.9074417365
3/9/2020 23:50:28	0.2367	1583812228	6.29477321	360.6639379	3.20619	0.9074725354

Epsilon Persei Results Table

Date	Velocity w/ Helio correction	EPOCH Time	Mean Anomaly	Deg	True Anomaly	Velocity
2/19/2020 3:14:41	22.1016	1582100081	8177.441887	468532.9073	177.55761	18.30736758
2/23/2020 2:02:27	15.2416	1582441347	8179.205797	468633.972	-142.27054	23.81144699
2/23/2020 2:07:54	26.5261	1582441674	8179.207488	468634.0688	-142.21758	24.47861941
2/23/2020 2:12:10	28.5569	1582441930	8179.208811	468634.1446	-142.17606	25.01788996
3/8/2020 0:53:34	25.0520	1583646814	8185.436526	468990.9664	-143.88648	25.74407793
3/8/2020 0:59:32	21.3480	1583647172	8185.438376	468991.0724	-143.83041	25.23405177
3/8/2020 1:03:58	21.2622	1583647438	8185.439751	468991.1512	-143.78868	24.87981004
3/9/2020 23:57:30	7.6341	1583812650	8186.293687	469040.0781	-104.97643	4.657089356
3/9/2020 0:02:05	4.4714	1583726525	8185.84853	469014.5725	-129.32693	3.992227884
3/9/2020 0:06:27	5.3957	1583726787	8185.849885	469014.6501	-129.27024	4.835165492

HIP26736 Results Table

Date	Velocity w/ Helio correction	EPOCH Time	Mean Anomaly	Deg	True Anomaly	Velocity
2/19/2020 2:53:03	39.4184403	1582098783	4236.777194	242749.452	162.11302	28.12034998
2/19/2020 2:54:55	36.67570854	1582098895	4236.777494	242749.4692	162.11812	28.40684734
2/23/2020 1:00:02	31.93995246	1582437602	4237.684534	242801.4387	175.62421	39.12568501
2/23/2020 1:05:09	29.1972207	1582437909	4237.685356	242801.4858	175.63543	39.36560844
2/23/2020 1:09:36	45.49707442	1582438176	4237.686071	242801.5268	175.64519	39.56879194
3/8/2020 1:12:58	-32.6420	1583647978	4240.925857	242987.1528	-81.85567	-29.70576041
3/8/2020 1:17:50	-30.8706	1583648270	4240.926639	242987.1976	-81.69256	-28.09474561
3/8/2020 1:22:20	-34.7461	1583648540	4240.927362	242987.2391	-81.54093	-27.96980544
3/8/2020 1:26:35	-25.4609	1583648795	4240.928045	242987.2782	-81.3976	-29.07128337
3/8/2020 1:30:50	-30.0321	1583649050	4240.928728	242987.3173	-81.25381	-31.34444911